Faraday Discussions

ARTICLE

Correlating structural dynamics and catalytic activity of AgAu nanoparticles with ultrafast spectroscopy and all-atom molecular dynamics simulations

Received 00th January 20xx,
Accepted 00th January 20xx

DOI: 10.1039/x0xx00000x

www.rsc.org/

G. F. Ferbonink,[a] T. S. Rodrigues,[b] D. P. dos Santos,[a] P. H. C. Camargo,[b] R. Q. Albuquerque,[c] and R. A. Nome[a]

In this study, we investigated hollow AgAu nanoparticles with the goal of improving our understanding of the composition-dependent catalytic activity of theses nanoparticles. AgAu nanoparticles were synthesized via the galvanic replacement method with controlled size and nanoparticle compositions. We studied extinction spectra with UV-Vis spectroscopy and simulations based on Mie theory and the boundary element method, and ultrafast spectroscopy measurements to characterize decay constants and the overall energy transfer dynamics as a function of AgAu composition. Electron-phonon coupling times for each composition were obtained from pump-power dependent pump-probe transients. These spectroscopic studies showed how nanoscale surface segregation, hollow interiors and porosity affect the surface plasmon resonance wavelength and fundamental electron-phonon coupling times. Analysis of the spectroscopic data was used to correlate electron-phonon coupling times to AgAu composition, and thus to surface segregation and catalytic activity. We have performed all-atom molecular dynamics simulations of model hollow AgAu core-shell nanoparticles to characterize nanoparticle stability and equilibrium structures, besides providing atomic level views of nanoparticle surface segregation. Overall, the basic atomistic and electron-lattice dynamics of core-shell AgAu nanoparticles characterized here thus aid the mechanistic understanding and performance optimization of AgAu nanoparticle catalysts.

Introduction

Recent advances in electron and optical microscopies have allowed high-resolution investigations of nanoparticle catalysts. For example, scanning transmission electron microscopy using energy dispersive X-ray tomography allowed detailed determination of three-dimensional compositional mapping of hollow AgAu nanoparticle catalysts, enabling the study of particle composition effects on surface segregation behavior and catalytic activity [1, 2]. Super-resolved single-molecule optical microscopy was used to image bimetallic PdAu nanoparticle catalysts with sub-particle spatial resolution [3]; nanoparticle imaging during catalysis towards the photodriven disproportionation reaction of resazurin to resorufin enabled the characterization of enhanced bimetallic activity of single nanocatalysts precisely at the PdAu interface. These studies have helped us understand mechanisms of nanoparticle catalysts from morphological and chemical information measured at high spatial resolution.

Ultrafast time-resolved spectroscopy allows the determination of fundamental molecular motions with atomic scale resolution in space and time. A large body of work on ultrafast spectroscopy studies of dynamics of metals (bulk and nanoparticle) has helped elucidate the main underlying energy relaxation mechanisms [4, 5].The specific decay time constants were found to depend on properties of the system under investigation. Nevertheless, a two-temperature model (TTM) is useful for describing energy transfer dynamics between electron cloud and metallic lattice in these systems [6]. In the TTM model, absorption of short light pulses creates a hot electron distribution, which cools by transferring energy to the lattice via electron-phonon coupling [7]. The lattice subsequently cools by transferring energy to the surrounding medium via phonon-phonon and acoustic mode relaxation. The TTM and continuum mechanics models are also consistent with first-principle calculations based on TD-DFT and molecular dynamics simulations of plasmonic materials, such as Au nanorods and Ag clusters [8,9].

Particularly relevant for the present work is the direct determination of electron-phonon coupling times from ultrafast spectroscopy measurements [4-6]. Within the context of characterizing metal nanoparticle catalysts, the experimental determination of electron-phonon couplings is potentially interesting, since this relaxation pathway occurs specifically at the nanoparticle surface/interface, which in turn is responsible for the nanoparticle catalytic activity. In this way, electron-phonon coupling times may be useful for correlating structural dynamics and catalytic activity of metal nanoparticles via ultrafast

[a] Instituto de Química, Universidade Estadual de Campinas (UNICAMP), Campinas-SP, Brazil. E-mail: nome@iqm.unicamp.br
[b] Departamento de Química Fundamental, Instituto de Química, Universidade de Sao Paulo, Av. Prof. Lineu Prestes, 748, 05508-000 São Paulo-SP, Brazil
[c] School of Pharmacy and Biomolecular Sciences, Liverpool John Moores University, Liverpool, UK. E-mail: R.Q.Albuquerque@ljmu.ac.uk

spectroscopy. We address this specific question in the present work for the particular case of hollow AgAu nanoparticle catalysts.

AgAu nanoparticles have been applied as catalysts towards a variety of transformations [10-17]. These include the reduction of 4-nitrophenol [10, 17], oxidation of alcohols [11], three-component coupling to form propargylamines [1], and the electrocatalytic oxygen reduction reaction [12]. They have also been employed together with semiconducting materials towards the photocatalytic water splitting [13]. Finally, as AgAu nanoparticles support surface plasmon resonant excitation, they are very attractive in the field of plasmonic catalysis [14, 15].

AgAu nanoparticles with controlled compositions have been synthesized by the galvanic replacement reaction with high efficiency and versatility [2]. Their formation mechanism has been recently investigated by optical and electron microscopies. Single-nanoparticle studies of the galvanic replacement reaction revealed that the transformation from Ag nanoparticle to AgAu nanocage is stochastic and occurs via an abrupt transition, which is limited by the formation of a nanosized void [16]. Electron microscopy characterization revealed the hollow and porous nature of these nanoparticles [1]. The resulting high-surface area was explored in catalysis and sensing applications [2, 17]. For example, composition-dependent catalytic activity was reported for these hollow AgAu nanoparticles towards a three-component coupling reaction forming propargylamine. The propargylamine yield varied nonlinearly as Au percentage yields increased from 0% to 100%, with maximum catalytic activity for an average composition of 18% Au. STEM EDX mapping showed that nanoparticle surface segregation of these hollow AgAu nanoparticles varies from Au-rich to alloyed to Ag-rich segregation as Au content increases from 5% to 75%. At 25% Au, the nanoparticles exhibited maximum Au surface coverage, thus highlighting the importance of nanoscale surface segregation for catalytic activity in this system.

In the present work, we present time-domain ultrafast spectroscopy and molecular dynamics simulations of hollow AgAu nanoparticles as a function of composition. The particles are synthesized by the galvanic replacement method and characterized by scanning electron microscopy and ICP-OES, as described previously. The linear optical properties of the hollow AgAu nanoparticles are characterized by UV-Vis spectroscopy and simulations based on Mie theory and the boundary element method. Ultrafast spectroscopy experiments are performed with the goal of understanding basic energy-relaxation mechanisms for these systems. Pump-probe spectroscopy transients with 100 fs time-resolution as a function of pump-pulse power are measured, and the resulting data is used to extract fundamental (intrinsic) electron-phonon coupling time constants as a function of AgAu nanoparticle composition. All-atom molecular dynamics simulations of model hollow AgAu core-shell nanoparticles complement the experimental results. The simulations are used to characterize nanoparticle stability and equilibrium structures as well as to provide atomic level characterization of nanoparticle surface segregation.

Results and discussion

Characterization

Figure 1 shows scanning electron microscopy (SEM) images of the hollow AgAu nanoparticles synthesized in the present work. The atomic percentages determined by ICP-OES are presented in Table 1.The chemical composition of the hollow AgAu nanoparticles shown in Figure 1 are: (B) $Ag_{85}Au_{15}$, (C) $Ag_{69}Au_{31}$, (D) $Ag_{67}Au_{33}$, (E) $Ag_{51}Au_{49}$, and (F) $Ag_{46}Au_{54}$, where the subscript denotes the mol % of each metal, and Figure 1A shows an SEM image of Ag NPs employed as chemical templates for their synthesis.

Table 1. Atomic percentages of Ag and Au in the hollow AgAu nanoparticles obtained by ICP-OES. The number in parenthesis denotes the concentration (in mM) for the corresponding $AuCl_4^-{}_{(aq)}$ solutions (2 mL) employed during the galvanic replacement reaction.

Insert Table 1 here

	Ag (mol %)	Au (mol%)	Sample
Au(0.2)	85	15	$Ag_{85}Au_{15}$
Au(0.4)	69	31	$Ag_{69}Au_{31}$
Au(0.5)	67	33	$Ag_{67}Au_{33}$
Au(0.6)	51	49	$Ag_{51}Au_{49}$
Au(0.8)	46	54	$Ag_{46}Au_{54}$

Insert Figure 1 here

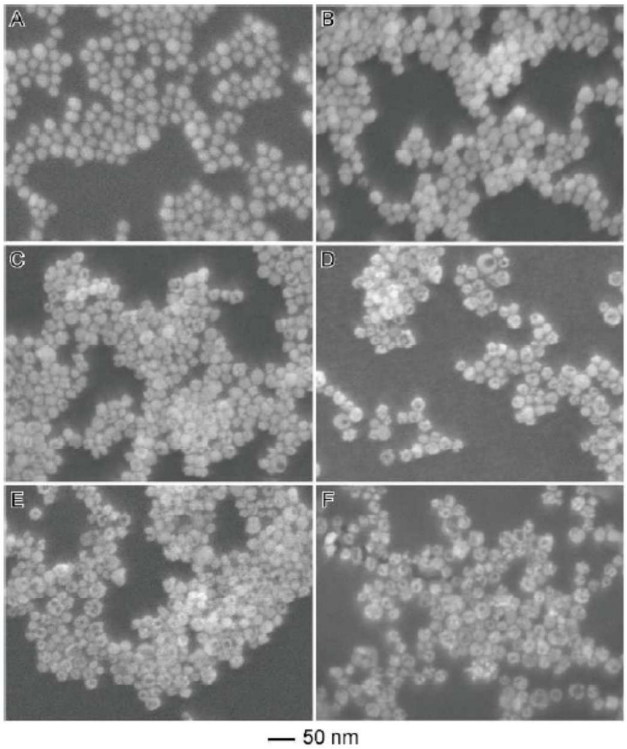

Figure 1. SEM images for hollow AgAunanoparticles obtained by the galvanic replacement reaction between Ag NPs (A) and different concentrations of 2 mL of $aAuCl_4^-{}_{(aq)}$ after 1 h following the addition of $AuCl_4^-{}_{(aq)}$ to a suspension containing Ag NPs and PVP. In B-F, the $AuCl_4^-{}_{(aq)}$ concentration corresponded to 0.2, 0.4, 0.5, 0.6, and 0.8 mM, respectively.

The overall size, shape and chemical composition given in Figure 1 and Table 1 are consistent with previous report[1,2].As can be clearly seen in Figures 1C-F, the bimetallic nanoparticles exhibit a porous structure with a hollow core and diameter of approximately40 nm, depending on the chemical composition of the bimetallic nanoparticle system. As previously reported, quantitative analysis of images measured with scanning transmission electron microscopy coupled with energy dispersive X-ray tomography allowed characterization of three-dimensional compositional variations of the nanoparticles, particularly atomic distribution at the nanoparticle surface and within the metallic portion of the nanoparticles[1]. As Au content increases, the hollow core size also increases, and the Ag and Au atoms occupy a smaller region of the entire nanoparticle volume. Furthermore, the atomic distribution at the nanoparticle surface is such that the nanoparticles exhibit Au-surface segregation at low %Au (up to approximately 25% Au), alloyed structure at the surface at intermediate Au% (up to approximately 50% Au), and Ag-surface segregation at higher Au mol%. Thus, it was demonstrated that the surface atomic composition of the hollow AgAu nanoparticles investigated here change from Au-surface coverage at low Au% to Ag surface coverage at higher Au%. Interestingly, the optimum catalytic performance of hollow AgAu nanoparticles in a three-component reaction producing propargylamine was correlated to maximum Au surface coverage rather than nanoparticle atomic percentages, thus exemplifying the challenge of characterizing nanoparticle catalysts[1].

Linear spectroscopy

Figure 2A shows experimental extinction spectra registered for the samples described in Table 1. The extinction spectrum of Ag nanoparticles (AgNP) is included for reference. All samples exhibit interband transitions in the UV, as shown in Figure 2A. Additionally, samples $Ag_{85}Au_{15}$, $Ag_{69}Au_{31}$, and $Ag_{67}Au_{33}$ exhibit surface plasmon resonance (SPR) bands at 418 nm, 455 nm, and 456 nm, respectively. These three samples also exhibit absorbance at longer wavelength, including broad SPR bands at 642 nm for samples $Ag_{69}Au_{31}$ and $Ag_{67}Au_{33}$, and a broad and weak absorbance tail that extends up to the near infrared for sample $Ag_{85}Au_{15}$. Samples $Ag_{51}Au_{49}$ and $Ag_{46}Au_{54}$ exhibit a predominant SPR band at 700nm and 800 nm, respectively. Overall, the samples investigated in the present work exhibit surface plasmon resonances spanning the visible and near infrared spectral ranges. At small Au atomic percentage (sample $Ag_{85}Au_{15}$), the extinction spectrum resembles that of Ag nanospheres. Starting with sample $Ag_{69}Au_{31}$, as the Au atomic percentage increases further, an additional surface plasmon resonance appears; this SPR band redshifts with increasing Au atomic percentage.

Insert Figure 2 here

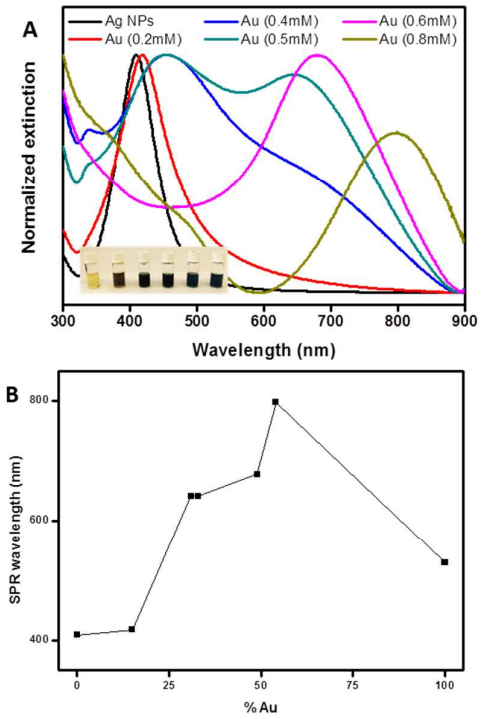

Figure 2 A Normalized extinction spectra recorded from aqueous suspensions containing the Ag NPs (black trace) and hollow AgAu nanoparticles obtained by employing different concentrations of a $AuCl_4^-{}_{(aq)}$ solution in the galvanic reaction as denoted by the values in parentheses. Inset photograph, from left to right: samples with increasing Au content. B Surface plasmon resonance wavelength as a function of %Au for hollow AgAu nanoparticles.

The optical properties of solid AgAu nanoparticles such as alloys and core-shell configurations generally exhibit SPR bands lying in between the SPR bands of pure Ag (410 nm) and Au (520 nm) nanospheres [18, 19]. The precise relationship between solid AgAu nanoparticle composition and SPR wavelength depends on nanoparticle configuration and the atomic mixing rule employed [16]. Nonetheless, to a first approximation, upon increasing the Au% in solid (not hollow) AgAu nanoparticles, the corresponding extinction spectrum exhibits SPR bands with wavelength that increases from 410 nm to 520nm. That is, the linear optical properties of solid AgAu nanoparticles can be accounted for in terms of nanoparticle stoichiometry.

In contrast, the results presented in Figure 2A show the appearance of SPR bands, such as λ_{SP} = 800 nm for $Ag_{46}Au_{54}$ composition, that extend well above the SPR wavelength of pure Au nanospheres due to the formation of hollow interiors. To further understand their linear optical properties, Figure 2B shows a plot of the measured SPR peak wavelength as a function of Au% in hollow AgAu nanoparticles investigated here, as obtained from Figure 2A. The SPR wavelength of AgNP and AuNP are also included for reference. Qualitatively, we observe a peaked curve with maximum SPR wavelength at intermediate 54% Au composition. The extent of SPR wavelength redshift observed for the hollow AgAu

nanoparticles investigated here suggests a complex interplay of structural, compositional and electronic factors that affect their optical properties and probably catalytic activity as well.

Mie theory and electrodynamics simulations

SPR redshift above that of spherical AuNP at 520 nm for hollow AgAu nanoshells has been reported previously [20, 21, and 22]. For instance, in reference [20] Goodman *et al* reported experimental results and simulations on the optical properties of hollow AgAu nanoshells with diameter less than 100 nm and exhibiting near infrared resonances. The theoretical model based on Mie theory and finite element electrodynamics modeling indicated that several factors contribute to the presence of a SPR band in the near infrared, including alloying, residual Ag in the nanoparticle core, nanoparticle porosity, and surface defects. In our case, as seen in Figure 1, the nanoparticles investigated here have complex shape with void size, nanoparticle porosity, and metallic component thickness that vary as a function of composition. In particular, they are not exactly hollow AgAu nanoshells, and it is challenging to describe precisely their overall shape. Nonetheless, we sought to investigate whether electrodynamics simulations based on Mie theory and the boundary element method can give further insights into the optical properties of the hollow AgAu nanoparticles investigated herein. Moreover, by employing simple model systems, we test whether basic structural and compositional features of the nanoparticles important for their catalytic activity may also affect their optical properties. To that end, we model the linear optical properties of our nanoparticles using phenomenological Mie theory with an effective medium description of spherical nanoparticle whereas a more realistic multi-layered shell particle geometry is investigated via electrodynamics modeling based on the boundary element method (see Computational Details section).

First, Mie theory was used to assess which volume fraction combination of Ag, Au, and water can be employed to give an effective medium description of the hollow AgAu nanoparticle that result in SPR resonances in the near infrared. Figure 3A shows the calculated extinction spectra of spherical particles with heterogeneous composition as a model system for hollow AgAu nanoparticles. More specifically, the dielectric function was modeled employing a weighted sum of tabulated complex dielectric constants for Ag and Au, in addition to the dielectric constant of water. For all systems investigated in Figure 3A, we use the same values of Ag/Au mol ratio as shown in Table 1, and we then include water with different volume fractions for each particle such that the calculated spectra give the trend observed experimentally. By using the three components (Ag, Au, and water) to calculate an effective particle dielectric constant, this approach accounts for porosity and compositional variation effects on the optical properties of hollow AgAu nanoparticles in a simple, systematic manner. Figure 3A shows that, as the fraction of Ag, Au, and water is varied, the surface plasmon resonance wavelength spans the entire spectral range from 400 nm to 800 nm, thus extending the SPR wavelength outside the range observed for spherical solid Au and AgAu nanoparticles [18, 19]. Comparing Figure 3A with Figure 2, we thus observe that the measured optical properties of hollow AgAu nanoparticles investigated here can be qualitatively accounted for using Mie theory.

Insert Figure 3 here

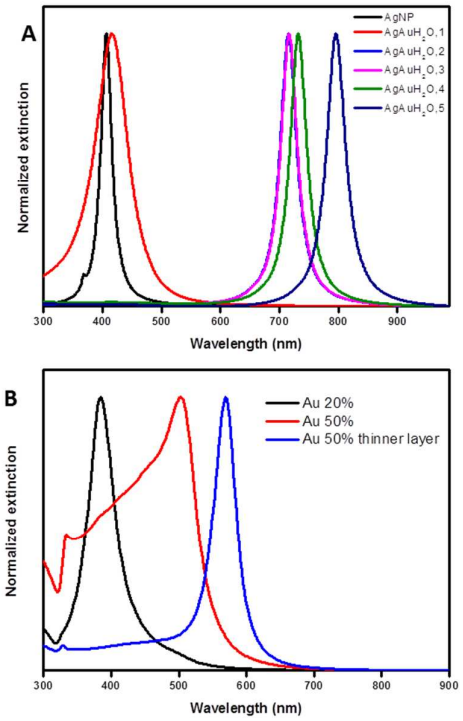

Figure 3 Mie theory and Boundary Element Method (BEM) modeling of hollow AgAu NPs. A: Normalized extinction spectra calculated with Mie theory for spherical nanoparticles at different volume fractions of Ag, Au and H_2O. B: Normalized extinction spectra calculated with BEM of systems "Au 20%", "Au 50%", and "Au 50% thin layer" (see Materials and Methods).

Previously, near infrared plasmonic resonances were observed in hollow AgAu nanoshells and modeled by incorporating 1 to 3 holes in the nanoshell structure [20]. Although our samples also exhibit hole-like features within their structure (see Figure 1 and reference [1]), surface segregation was used to explain the main morphological and compositional observations from electron microscopy images and correlation to catalytic activity. Specifically, as shown more clearly in reference [1], with increasing Au%, nanoparticle surface segregation inverts from Au-rich to Ag-rich, and maximum Au surface coverage was observed for nanoparticles with approximately 25-30% Au, which also was found to correlate to the optimal catalytic performance of the AgAu nanoparticles. Therefore, we performed boundary element method electrodynamics simulations with a model varying surface composition rather than the presence of holes, with the aim of gaining further insights into the role of surface composition effects in hollow AgAu nanoparticles on their optical properties and catalytic activity.

Figure 3B shows extinction spectra calculated with the BEM method for spherical geometry containing water at the center and sequential layers/shells composed of Ag and/or Au to match the chemical mapping of hollow AgAu nanoparticles reported previously [1]. The "Au 20%" model system is a spherical particle with 40 nm diameter and water-Ag-Au structure, with water at the center and two consecutive layers of Ag and Au. In connection with reference [1], this a model that exhibits Au surface segregation (see Materials and Methods). As shown in Figure 3B, this model resulted in an extinction spectrum with SPR resonance at 410 nm, which is similar to that observed experimentally for hollow bimetallic nanoparticle with $Ag_{85}Au_{15}$ composition and Au surface segregation. The "Au 50%" model has a water-Au-Ag structure, and thus with Ag surface segregation. As shown in Figure 3B, the resulting extinction spectrum exhibits a predominant SPR resonance near 520 nm, as in the case of spherical solid Au nanoparticles. Using the current approach, it was not possible to extend the SPR wavelength beyond 520 nm by tuning geometrical parameters of the model alone (not shown). Finally, the "Au 50% thin layer" model has a structure composed of water-Ag-Au-Ag. That is, this model is similar to the model "Au 50%" and with 50% Au composition and Ag surface segregation, although it also has an additional Ag sublayer structure to match the experimentally observed compositional variation [1]. The extinction spectrum observed for this geometry, shown in Figure 3B, has a SPR wavelength at 600 nm, above the SPR wavelength of Au NPs. A better correlation to the experimental spectra at higher Au content can be achieved by reducing the metal layer (at the same proportion), which is also a simplified approximation to describe a porous surface. However, considering that the outer layer already has 1.5 nm thickness, reducing it further may require non-local dielectric constant for reliable computation of their optical properties. Alternatively, further shift of the SPR resonance to the near infrared may also be obtained by adding hole-like features to the model. However, we note that the three-layered structures that match the morphological and compositional variations observed experimentally already gives SPR wavelengths outside the range of SPR wavelength of pure AgNP and AuNP, thus being qualitatively consistent with our experimental results. Overall, the model systems investigated here are useful for understanding the compositional variations and surface segregation observed in the linear optical properties of hollow AgAu nanoparticles, and probably serve as good model systems to understand their nonlinear optical properties also.

Ultrafast spectroscopy

Ultrafast pump-probe spectroscopy measurements of hollow AgAu nanoparticles in aqueous solution were performed to characterize electron-phonon interactions and study their variation as a function of hollow AgAu nanoparticle composition and morphology. Figures 4A-D show the ultrafast spectroscopy data set measured in the present work, including pump-probe transients as a function of pump power as well as nanoparticle composition: (A) $Ag_{46}Au_{54}$, (B) $Ag_{51}Au_{49}$, (C) $Ag_{67}Au_{33}$, (D) $Ag_{69}Au_{31}$. Each transient is analyzed to obtain relaxation time constants (see Experimental Details section), whereas the pump-power dependent time constants are used to obtain values for electron-phonon coupling times at zero pump power.

Insert Figure 4 here

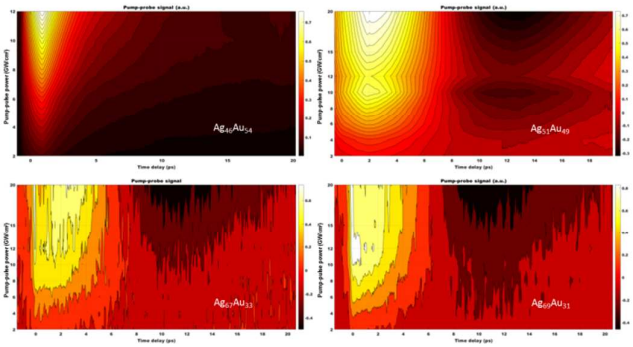

Figure 4. Ultrafast pump-probe signals for (A) $Ag_{46}Au_{54}$, (B) $Ag_{51}Au_{49}$, (C) $Ag_{33}Au_{67}$, and (D) $Ag_{31}Au_{69}$. Each figure shows pump-probe transients recorded at the indicated pump pulse power.

The results shown in Figure 4 are consistent with a large body of work on ultrafast spectroscopy of metal nanoparticles of varying size, shape, and chemical composition, including bimetallic nanoparticles such as AgAu[4,5,23]. Thus, we follow these references in the data analysis and interpretation of the ultrafast spectroscopy signals. Generally, the ultrafast response of metal nanoparticles is described by four prominent features: electron-electron scattering, electron-phonon coupling, phonon-phonon relaxation, and nanoparticle acoustic oscillations coupled to phonon-environment coupling (see Figure 5A). The relaxation mechanism is well described by a two-temperature model whereby light absorption by the nanoparticle creates a hot electron distribution, which transfers heat to the lattice within a few picoseconds [4-6]. Impulsive lattice heating drives nanoparticle acoustic oscillations and energy transfer to the surrounding medium. This mechanism for optical dynamics of metal nanoparticles was used to describe our results shown in Figures 4A-D.

Figure 5A shows time-resolved ultrafast pump-probe signals for sample $Ag_{46}Au_{54}$ up to 20 ps (same data as in Figure 4A). We have also measured pump-probe signals up to 100 ps time delay and with up to 240 GW/cm^2 pump power (not shown) but our focus here is on the determination of electron-phonon coupling times in the lower-power limit. From a nonlinear least squares fit to the data (see Experimental Details section), the main features of the ultrafast pump-probe signal are an instantaneous response at time zero, two exponential decays with ~300 fs and ~3 ps time constants, respectively, and an exponentially decaying oscillation with ~20 ps period and ~10 ps time constant (actual values of electron-phonon decay constants for each pump power are shown in Figure 5B).

Insert Figure 5 here

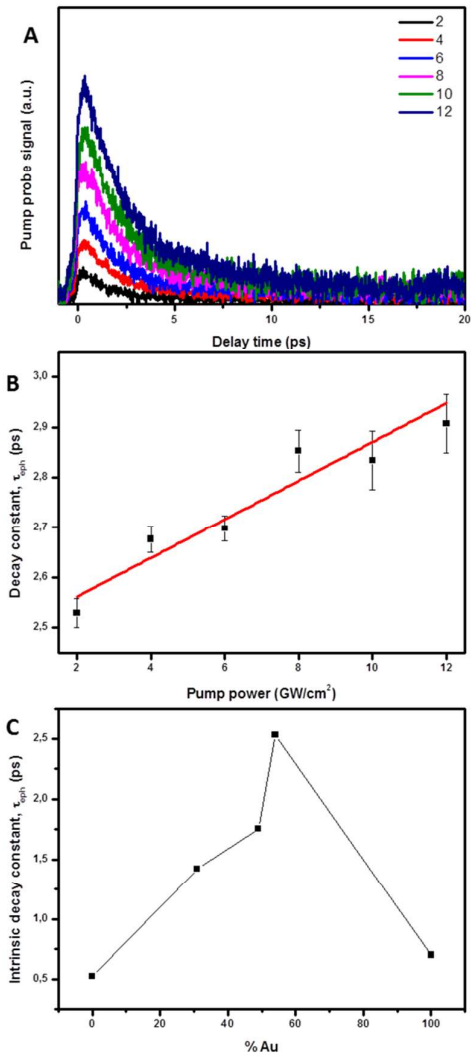

Figure 5 Analysis of ultrafast spectroscopy data shown in Figure 4. A. Pump-probe data shown in Figure 4A. B. Electron-phonon coupling times (black points) as a function of pump power for sample $Ag_{46}Au_{54}$. The solid red line is a linear fit to the data. C. Electron-phonon coupling times as a function of %Au for hollow AgAu nanoparticles.

In the present work, our focus is on the characterization of electron-phonon time constants and how it varies as a function of hollow AgAu nanoparticle composition. Electron-phonon time constants inform on the coupling and energy transfer between the nanoparticle electron cloud and structure. Electron-phonon interactions are sensitive to surface features, including nanoscale segregation, and thus may be used to correlate with catalytic activity. Furthermore, extinction spectra (measurements and simulations) probe the optical properties of nanomaterials based on their dielectric response, whereas molecular dynamics simulations provide information on atomic scale structural (lattice) changes occurring on the femtosecond to picosecond time scale. Thus, electron-phonon coupling times may be used to connect the structure, linear spectroscopy and molecular dynamics simulation results presented here.

Figure 5B shows our data analysis of electron-phonon time constants for sample $Ag_{46}Au_{54}$. The left figure shows the ultrafast response at early times, which is primarily composed of electron-electron scattering and electron-phonon coupling. After light absorption and electron thermalization, the electrons return to the local equilibrium solely by electron-phonon processes. Ultrafast spectroscopy thus uniquely probes this relaxation pathway, whereas transport experiments measure a combined rate caused by all available relaxation mechanisms. We fitted the pump-power dependence of the ultrafast response of $Ag_{46}Au_{54}$ as described above, and Figure 5B shows a plot of electron-phonon time constants as a function of pump power for sample $Ag_{46}Au_{54}$. We note that the results shown in Figure 5B are for pump pulse power in the zero power limit. Fitting the data shown in Figure 5B to a straight line gives an intercept equal to τ_{eph}^{0}, which is the fundamental electron-phonon coupling time constant at zero pump power. This analysis allows extraction of electron-phonon interactions in the absence of light excitation (continuous or impulsive) and correspond to an intrinsic property of the nanomaterial. The electron-phonon coupling times retrieved are temperature-independent in the 23 ^{o}C - 90 ^{o}C range (not shown). Therefore, ultrafast spectroscopy allows the characterization of metal nanoparticle catalyst properties that are relevant for catalysis even in the absence of any photo-driven or plasmonic effects.

Figure 5C shows the zero-power limit electron-phonon relaxation times calculated as described in Figure 5B for four samples: $Ag_{69}Au_{31}$, $Ag_{67}Au_{33}$, $Ag_{51}Au_{49}$, and $Ag_{46}Au_{54}$. We were unable to measure pump-probe signals for sample $Ag_{85}Au_{15}$ because this sample does not absorb light in the near-infrared wavelength of the laser used in the resonant one-color pump-probe experiments described here. Samples $Ag_{69}Au_{31}$, $Ag_{67}Au_{33}$, $Ag_{51}Au_{49}$ exhibit broad SPR resonances in 670-700nm range and significant light absorption at 800 nm. We note that our pump-probe transients exhibit acoustic oscillation signals in all samples (see Figures 4B-D), which is indicative of high sample quality and low polydispersity.

The fundamental (zero power limit) electron-phonon relaxation times for pure Ag and Au and solid AgAu nanoparticle alloy are included in Figure 5C for reference. The ultrafast dynamics of solid AgAu alloys have been investigated previously [18], showing a linear dependence of electron phonon coupling time on %Au (mole fraction). The electron-phonon coupling times of bimetallic nanoparticle alloys correspond to an average of the electron-phonon coupling times of each componentetal, weighted by the density of electronic states from each metal[6,24]. In the case of solid AgAu nanoalloys, this approach reduces to weighting of τ_{eph} according to sample stoichiometry[25], as was performed in the ultrafast spectroscopy analysis of AgAu nanoalloys described in [23].

Figure 5C shows that the zero power limit electron-phonon coupling times of the hollow AgAu nanoparticles investigated here exhibit a nonlinear dependence on %Au, with longer coupling times at a composition (54% Au) in between that of bulk Ag and Au.

Qualitatively, the shape of the curve in Figure 5C resembles that observed for composition-dependent SPR wavelength of these nanoparticles, Figure 2B. Thus, both linear optical properties and electron-phonon interactions depend nonlinearly on sample stoichiometry. Based on Mie theory and BEM method calculations described above, we attributed the differences in SPR wavelength between hollow and solid AgAu nanoparticles to a complex interplay of alloying, porosity, and nanoscale segregation [20]. Likewise, we believe these factors may be responsible for the observed composition dependence of the electron-phonon coupling times.

Since electron-phonon coupling occurs by phonon emission, we may think of the measured electron-phonon coupling times as arising from the interaction between an individual primary Brownian oscillator in a hot quantum state coupled to a bath of non-interacting oscillators representing the lattice. In this picture, dissipation is governed by a frictional term described by the spectral density of lattice phonon modes. The overdamped dissipation of hot electron distribution observed in our ultrafast spectroscopy measurements is consistent with an Ohmic form for the bath spectral density, thus supporting our use of a system plus reservoir description of relaxation to equilibrium. Therefore, the longer electron-phonon relaxation times measured for intermediate values of %Au are indicative of smaller coupling between populated electronic states near the Fermi level and the lattice for hollow AgAu nanoparticles compared to AgAu nanoalloys or bulk Ag and Au. We thus suggest that increasing Au content of bimetallic hollow AgAu nanoparticles investigated here introduces a frequency cutoff in the spectrum of energy accepting lattice phonon modes due to increasing void size and Ag surface segregation at higher Au content. Conversely, to connect the ultrafast spectroscopy results with catalytic activity, we note that the catalytic activity increases as Au content decreases in the Au% range investigated here (between 15% Au and 54% Au). The measured electron-phonon coupling times decrease with decreasing Au content, and thus we may correlate Au surface segregation and decreasing void size with greater friction responsible for coupling of the electron density with the atomic lattice. Although no catalytic reactions per se have been investigated in the present manuscript, the fundamental relaxation processes characterized herein are useful for understanding catalysis. The time-resolved data was used to characterize the zero power limit (in the absence of light) of electron-phonon coupling times, which in turn correspond to the fundamental motions and interactions the nanoparticle undergoes during any thermal process (i.e., fluctuation-dissipation theorem), such as the catalytic reactions described in references [1, 2].

Molecular Dynamics simulations

Atomistic Molecular Dynamics (MD) simulations were performed for some investigated nanoshells to get insight on the spatial distribution of Au and Ag, as well as on the overall stability of the nanoshell. The embedded atom model [26] was used in the MD simulations since it has successfully described properties of metallic nanoparticles [19, 27]. The simulations were run using the lammps package [28] and the NVT ensemble. The simulated AgAu nanoshells (20% Au alloyed, 20 % Au as $Ag_{shell}Au_{core}$, and 54% Au alloyed) contained ca $86x10^3$ atoms and had external (internal) diameter of about 15 nm(7 nm).

Initial tests were carried out for the 20% Au systems to compare the relative stability of core shell versus alloy (Fig. 6a), which are common structures observed for AgAu systems [19].The nanoshell is more stabilized when alloyed, and the melting point of the nanoshell occurs about 30 K later for the alloyed structure, at ca 1080 K, when the nanoshell also implodes (Fig. 6e). Also, the nanoshell's surface becomes more Ag-rich at higher temperatures (see the insets inside Fig. 6a), which agrees with another study on AgAu nanoparticles showing that Au atoms tend to stay in the core regions, while Ag prefers the shell ones [19]. The alloyed structure was then adopted for the remainder MD simulations.

The annealing of the alloyed nanoshell via heating up to 900 K and cooling down slowly (in 10 ns) to 300 K reveals that both the internal and external surfaces are Ag-rich, as shown by the radial distributions of Au and Au (Fig. 6b)calculated for the composition 20 % Au. For 54 % Au, the surface was also found to be more Ag-rich. In Fig. 6b, the ratio between the heights of the Ag and Au signals at the surface are always larger than the composition-based value of 4, which is also true for the 54 %Au composition.

The snapshots of the annealed structure of the alloyed nanoshells are shown in Figs. 6c (20% Au) and 6d (54 % Au), which indicate that few Au atoms on the surface might nucleate to form small islands where catalytic activity is known to be stronger, but regions containing single Au atoms might also contribute to the catalytic activity. The composition of 20 % Au corresponds to the optimum composition for catalysis of these particles, which reveals that very small Au clusters might be necessary to achieve a good catalytic activity (compare Figs. 6c and 6d). In general, Au atoms did not change the surface structure when they replaced Ag atoms on any Ag-rich surfaces, which is due to a very similar lattice constant of both pure metals. The facets of the nanoshell could be associated with the Miller indices 100 or 111, although mostly 111 planes can be seen in Figs 6c,d.Interestingly, Au has shown a slightly higher tendency for segregating into small Au islands in the case of 111 facets. The temperature-dependent snapshots of the internal and external surface of the alloyed nanoshell (20 % Au) is also shown in Fig. 6e, which correspond to the blue curve shown in Fig. 6a.

Insert Figure 6 here

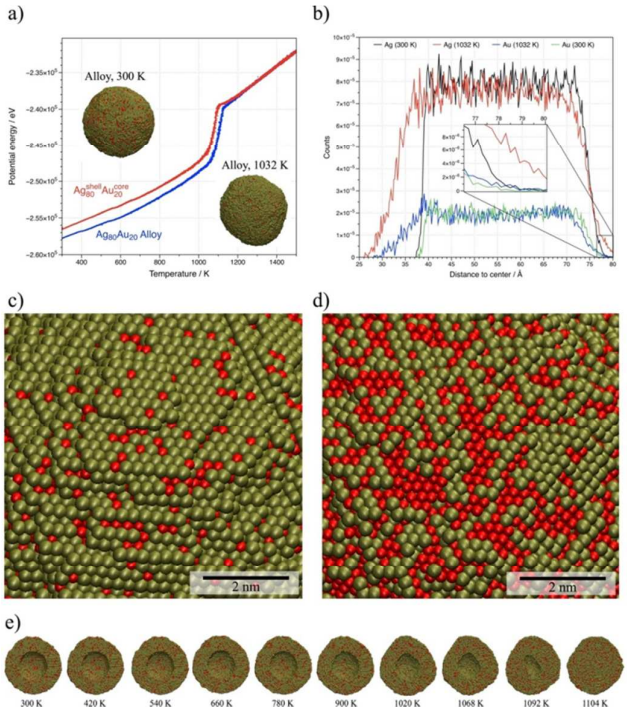

Figure 6. (a) Melting curves for alloyed (blue) and AgshellAucore (red) nanoshells with 20% Au. (b) Radial distribution of Au and Ag in alloyed nanoshells with 20 % Au. Snapshots of the annealed alloyed nanoshells with 20 % Au (c) and 54 % Au (d) at 300 K. (e) Melting sequence of the alloyed nanoshell with 20 % Au, corresponding to the blue curve shown in (a). Color code: Au = red.

Conclusions

In conclusion, we have investigated hollow AgAu nanoparticles synthesized via the galvanic replacement method with controlled size and nanoparticle compositions. Extinction spectra were characterized by UV-Vis spectroscopy and simulations based on Mie theory and the boundary element method. Ultrafast spectroscopy measurements enabled the characterization of decay constants for these nanoparticles, and the overall energy transfer dynamics is consistent with previous work on metal nanoparticles. Electron-phonon coupling times for each composition were obtained from pump-power dependent pump-probe transients. These spectroscopic studies showed how nanoscale surface segregation, hollow interiors and porosity affect the surface plasmon resonance wavelength and fundamental electron-phonon coupling times as a function of nanoparticle composition. All-atom molecular dynamics simulations of model hollow AgAu core-shell nanoparticles allowed characterization of nanoparticle stability and equilibrium structures, besides providing atomic level views of nanoparticle surface segregation. Overall, the results presented herein provided time-resolved and atomic level insights on surface segregation. Previously, composition-dependent catalytic activity of hollow AgAu core-shell nanoparticles was correlated to surface segregation [1, 2]. Herein, the spectroscopic measurements as a function of composition were also correlated to surface segregation and catalytic activity. Thus, we envision that these findings can aid the mechanistic understanding and performance optimization of AgAu nanoparticle catalysis as well as inspire the development of novel catalysts with targeted performances towards a myriad of transformations. Finally, the approach described herein may be extended to other bimetallic and catalytic nanoparticle combinations.

Experimental and computational details

Materials and Methods

Analytical grade silver nitrate ($AgNO_3$, 99%, Sigma-Aldrich), polyvinylpyrrolidone (PVP, Sigma-Aldrich, M.W. 55,000 g/mol), polyvinylpyrrolidone (PVP, Sigma-Aldrich, M.W. 10,000 g/mol), Ethylene glycol (EG, 99.8%, Sigma-Aldrich), Tetrachloroauric(III) acid trihydrate ($HAuCl_4.3H_2O$, ≥99.9%, Sigma-Aldrich), were used as received. The scanning electron microscopy (SEM) images were obtained using a JEOL field emission gun microscope JSM 6330F operated at 5 kV. The samples were prepared by drop-casting an aqueous suspension containing the nanostructures over a silicon wafer, followed by drying under ambient conditions. UV-Vis spectra were obtained from aqueous suspensions containing the nanostructures with a Shimadzu UV-1700 spectrophotometer. The Ag and Au atomic percentages were measured by inductively coupled plasma optical emission spectrometry (ICP-OES) using a Spectro Arcos equipment.

Synthetic Procedures

Synthesis of Ag seeds. Ag seeds were prepared by the polyol process. In a typical experiment, 5 mg of polyvinylpyrrolidone (PVP) was dissolved in 37.5 mL of ethylene glycol. Then, $AgNO_3$ (200 mg, 1.2 mmol) was added and mixed until the complete dissolution. The resulting solution was heated to 125 °C for 2.5 hours, leading to the appearance of a greenish-yellow color, allowed to cool down to room temperature, and diluted to 125 mL of water.

Synthesis of hollow AgAunanoparticles. The syntheses of hollow AgAu nanoparticles were performed as described previously [1]. The syntheses of hollow AgAu nanoparticles were based on the galvanic replacement reaction between performed Ag nanospheres and $AuCl_{4\,(aq)}^-$ precursor. In a typical run, a mixture containing 5 mL of PVP (M.W. 55,000 g/mol) aqueous solution (0.1 wt %) and 1 mL of as-prepared suspension containing the Ag nanospheres was stirred at 100 °C for 10 min in a 25 mL round-bottom flask. Then, 2 mL of $AuCl_{4\,(aq)}^-$ precursor (0.2, 0.4, 0.5, 0.6, and 0.8 mM) was added dropwise and the reaction allowed to proceed at 100 °C for another 1 h.

Simulations

Absorption spectrum modelling. Mie theory simulations of extinction spectra were performed employing the effective medium

approximation [29,30], in which the nanoparticles were modeled as a compositional mixture of Ag, Au, and H_2O with an effective dielectric constant given by the formula

$$\sum f_i \frac{\varepsilon_i - \varepsilon_{eff}}{\varepsilon_{eff} + g(\varepsilon_i - \varepsilon_{eff})} = 0, \qquad \sum f_i = 1$$

where ε_1 and ε_2 are the dielectric functions of the constituent materials (Ag, Au, and H_2O in our case). The coefficient f_1 represents the volume fraction of each material in the mixture, with the remaining material comprising a fill fraction such that their sum equals one. The constant *g* is a geometric factor that equals 1/3 for spherical inclusions.

The extinction spectra were also simulated by the boundary element method approach (BEM) [31, 32], using the MNPBEM Toolbox from Matlab. The nanoparticles were modeled as water-filled hollow bimetallic shells. The three structures used in BEM calculations were created by adding successive layers of the materials from the compositional mixture, starting from the origin, as follows: (A) Au 20%: H_2O (2.5 nm radius), Ag (16 nm thick shell) and Au (1.5 nm thick shell); (B) Au 50%: H_2O (10 nm radius), Ag (2.2 nm thick shell), Au (5.6 nm thick shell) and Ag (2.2 nm thick shell); (C) Au 50%_r15: H_2O (15 nm radius), Ag (1.2 nm thick shell), Au (2.6 nm thick shell) and Ag (1.2 nm thick shell). In all electrodynamics simulations described in the present work, the optical properties of bulk silver [33] and gold [34] metals were used.

Molecular Dynamics simulations. Molecular Dynamics (MD) simulations were carried out using the embedded atom model (EAM, [26] and the lammps program [28]. The NVT ensemble was adopted and the system was initially equilibrated at 1K. All visualizations were done using the VMD program [35] and computations were run in a MacPro computer (24 processors). The composition $Ag_{46}Au_{54}$ was simulated to match the experiment, as well as the outer/inner radius ratio of 2 for the simulated nanoshells.

Ultrafast Spectroscopy. The pump-probe experiments were carried out as described previously [36]. Briefly, 70 fs pulses from a Ti:sapphire laser are split into pump (90%) and probe (10%) beams. A 40 cm focal-length lens was used to focus both pump and probe beams on the sample, and the time delay between beams is controlled by a computer-controlled motorized delay stage. The pulse duration was characterized at the sample position by frequency-resolved optical gating. The sample was placed on a manual xyz-linear translation stage, which was kept fixed in position during the ultrafast experiments. To enhance the signal detection sensitivity, we have used a combination of lock-in amplifier and an optical chopper. The measured signals are fitted by a convolution of the material response function with the instrument response function. The response function, in turn, is a convolution of the Heaviside step function with three exponential decays describing electron-electron scattering, electron-phonon coupling, and phonon-phonon relaxation, an exponentially decaying component accounting for the acoustic oscillation component. These parameters are determined by nonlinear least squares fitting [36].

Conflicts of interest

There are no conflicts to declare.

Acknowledgements

We gratefully acknowledge financial support from FAPESP (grant numbers 16/23430-9 (RAN), 15/21366-9 and 15/26308-7 (PHCC)) and CNPq(grant numbers 408985/2016-0 (DPS) and 01300.008995/2017-91 (RAN)).

References

1 T. J. A. Slater, A. Macedo, S. L. M. Schroeder, M. G. Burke, P. O'Brien, P. H. C. Camargo, and S. J. Haigh, *Nano Lett.*, 2014, **14**, 1921.
2 A. G. M. Silva, T. S. Rodrigues, S. J. Haigh, and P. H. C. Camargo, *Chem. Commun.*, 2017, **53,**7135.
3 G. Chen, N. Zou, B. Chen, J. B. Sambur, E. Choudhary, and P. Chen, *ACS Central Science*, 2017, **3**, 1189.
4 A. Crut, P. Maioli, F. Vallée, and N. Del Fatti, *J. Phys.: Condens. Matter*, 2017, **29**, 123002.
5 G.V. Hartland, *Chem. Rev.*, 2011, **111**, 3858.
6 R. W. Schoenlein, W. Z. Lin, and J. G. Fujimoto, *Phys. Rev. Lett.*, 1987, **58**, 1680.
7 P. B. Allen, *Phys. Rev. Lett.*, 1987, **59**, 1460.
8 C. M. Lethiec, L. R. Madison, and G. C. Schatz, *J. Phys. Chem. C*, 2016, **120**, 20572.
9 Y. Gan, Z. Sun, and Z. Chen, *Phys. Chem. Chem. Phys.*, 2016, **18**, 22590.
10 P. Hervés, M. Pérez-Lorenzo, L. M. Liz-Marzán, J. Dzubiella, Y. Lu, and M. Ballauff, *Chem. Soc. Rev.*, 2012, **41**, 5577.
11 T. Shirman, J. Lattimer, M. Luneau, E. Shirman, C. Reece, M. Aizenberg, R. J. Madix, J. Aizenberg, and C. M. Friend, *Chem. Eur. J.*, 2017, **23**, 1.
12 P. Hu, Y. Song, L. Chen, and S. Chen, *Nanoscale*, 2015, **7**, 9627.
13 A. A. Melvin, K. Illath, T. Das, T. Raja, S. Bhattacharyya, and C. S. Gopinath, *Nanoscale*, 2015, **7**, 13477.
14 J. L. Wang, R. A. Ando, and P. H. C. Camargo, *ACS Catal.*, 2014, **4**, 3815.
15 T. S. Rodrigues, A. G. M. da Silva, A. B. L. de Moura, I. G. Freitas, and P. H. C. Camargo, *RSC Adv.*, 2016, **6**, 62286.
16 J. G. Smith, Q. Yang, and P. K. Jain, *Angew. Chem. Int. Ed.*, 2014, **126**, 2911.
17 M. V. Petri, R. A. Ando, and P. H. C. Camargo, *Chem. Phys. Lett.*, 2012, **531**, 188.
18 S. Link and M. A. El-Sayed, *J. Phys. Chem. B*, 1999, **103**, 8410.
19 J. F. Gomes, A. C. Garcia, C. Pires, E. B. Ferreira, R. Q. Albuquerque, G. Tremiliosi-Filho, and L. H. S. Gasparotto, *J. Phys. Chem. C*, 2014, **118**, 28868.
20 A. M. Goodman, Y. Cao, C. Urban, O. Neumann, C. Ayala-Orozco, M. W. Knight, A. Joshi, P. Nordlander, and N. J. Halas, *ACS Nano*, 2014, **8**, 3222.
21 A. Shakiba, S. Shah, A. C. Jamison, I. Rusakova, T.-C. Lee, and T. R. Lee, *ACS Omega*, 2016, **1**, 456.
22 M. V. Petri, R. A. Ando, and P. H. C. Camargo, *Chem. Phys. Lett.*, 2012, **531**, 188.
23 M. Broyer, E. Cottancin, J. Lermé, M. Pellarin, N. Del Fatti, F. Vallée, J. Burgin, C. Guillon, and P. Langot, *Faraday Discuss.*, 2008, **138**, 137.
24 A. Comin, K. Korobchevskaya, C. George, A. Diaspro, and L. Manna, *Nano Lett.*, 2012, **12**, 921.
25 Z. Lin, L. V. Zhigilei, and V. Celli, *Phys. Rev. B*, 2008, **77**, 075133.

26 M. S. Daw and M. Baskes, Phys. Rev. B: Condens. Matter Mater. Phys., 1984, 29, 6443.
27 T. Schmidt, R. Q. Albuquerque, R. Kempe, and S. Kümmel, *Phys. Chem. Chem. Phys.*, 2016, **18**, 31966.
28 S. Plimpton, J. Comput. Phys., 1995, 117, 1.
29 Z. Shi, G. Piredda, A. C. Liapis, M. A. Nelson, L. Novotny, and R. W. Boyd, *Opt. Lett.*, 2009, **34**, 3535.
30 X. Zeng, D. Berkman, P. Hui, and D. Stroud, *Phys. Rev. B*, 1988, **38**, 10970.
31 Hohenester, U.; Trügler, A. *Comput. Phys. Commun.***2012**, *183* (2), 370.
32 García de Abajo, F. J.; Howie, A. *Phys. Rev. B - Condens. Matter Mater. Phys.***2002**, *65* (11), 1154181.
33 Palik, E. D. *Handbook of Optical Constants of Solids*; Academic Press, 1985.
34 Johnson, P. B.; Christy, R. W. *Bull. Am. Phys. Soc.***1971**, *16* (7), 785.
35 Humphrey, W., Dalke, A. and Schulten, K., "VMD - Visual Molecular Dynamics", J. Molec. Graphics, 1996, 14, 33.
36 G. F. Ferbonink, E. R. Spada, D. P. dos Santos, M. L. Sartorelli, and R. A. Nome, *J. Braz. Chem. Soc.*, 2016, **27**, 423.